

Polymeric microneedle-mediated transdermal delivery of melittin for rheumatoid arthritis treatment

Du, Guangsheng ; He, Penghui; Zhao, Jiaxuan; He, Chunting; Zhang, Zhihua; Zhang, Zhibing; Sun, Xun

DOI:

[10.1016/j.jconrel.2021.07.005](https://doi.org/10.1016/j.jconrel.2021.07.005)

License:

Creative Commons: Attribution-NonCommercial-NoDerivs (CC BY-NC-ND)

Document Version

Peer reviewed version

Citation for published version (Harvard):

Du, G, He, P, Zhao, J, He, C, Zhang, Z, Zhang, Z & Sun, X 2021, 'Polymeric microneedle-mediated transdermal delivery of melittin for rheumatoid arthritis treatment', *Journal of Controlled Release*, vol. 336, pp. 537-548. <https://doi.org/10.1016/j.jconrel.2021.07.005>

[Link to publication on Research at Birmingham portal](#)

General rights

Unless a licence is specified above, all rights (including copyright and moral rights) in this document are retained by the authors and/or the copyright holders. The express permission of the copyright holder must be obtained for any use of this material other than for purposes permitted by law.

- Users may freely distribute the URL that is used to identify this publication.
- Users may download and/or print one copy of the publication from the University of Birmingham research portal for the purpose of private study or non-commercial research.
- User may use extracts from the document in line with the concept of 'fair dealing' under the Copyright, Designs and Patents Act 1988 (?)
- Users may not further distribute the material nor use it for the purposes of commercial gain.

Where a licence is displayed above, please note the terms and conditions of the licence govern your use of this document.

When citing, please reference the published version.

Take down policy

While the University of Birmingham exercises care and attention in making items available there are rare occasions when an item has been uploaded in error or has been deemed to be commercially or otherwise sensitive.

If you believe that this is the case for this document, please contact UBIRA@lists.bham.ac.uk providing details and we will remove access to the work immediately and investigate.

1 **Polymeric microneedle-mediated transdermal delivery of melittin for rheumatoid arthritis treatment**

2 Guangsheng Du¹, Penghui He¹, Jiaxuan Zhao¹, Chunting He¹, Min Jiang¹, Zihua Zhang², Zhibing Zhang²,
3 Xun Sun^{1*}

4 ¹ Key Laboratory of Drug-Targeting and Drug Delivery System of the Education Ministry, Sichuan
5 Engineering Laboratory for Plant-Sourced Drug and Sichuan Research Center for Drug Precision
6 Industrial Technology, West China School of Pharmacy, Sichuan University, Chengdu, 610064, PR China

7 ² School of Chemical Engineering, University of Birmingham, Edgbaston, Birmingham, B15 2TT, UK

8
9 *Corresponding author

10 E-mail address: sunxun@scu.edu.cn

11

12 **Abstract**

13 Transdermal drug delivery systems for rheumatoid arthritis (RA) have been receiving increasing
14 attention as they can potentially overcome drawbacks which exist in traditional oral or injection
15 strategies, including low patient compliance and serious gastrointestinal side effects. However,
16 transdermal delivery of RA drugs especially biological drugs suffers from low drug delivery efficiency due
17 to the robust skin barrier. Herein, we fabricated melittin-loaded hyaluronic acid (HA) microneedles and
18 investigated their capacity for inhibiting RA. We showed that melittin-loaded HA microneedles
19 possessed high mechanical strength for successful delivery of melittin into the skin and effectively
20 inhibited RA progression in adjuvant induced both rodent and murine models, as shown by results in
21 histological, paw swelling and arthritis score. Furthermore, after modifying HA with cross-linkable
22 groups, the fabricated microneedles with sustained release properties could further improve the
23 therapeutic potency. Cytokine and T cell analysis in the paws and lymphatic organs indicated that the
24 application of microneedles suppressed the levels of pro-inflammation cytokines including IL-17 and
25 TNF- α , and increased the percentage of regulatory CD4 T cells. Our study revealed that polymeric
26 microneedle-mediated transdermal delivery of melittin could serve as a new therapy with high
27 compliance and good therapeutic efficacy for RA and other autoimmune diseases.

28 **Keywords:** Polymeric microneedles; Melittin; Rheumatoid arthritis; Sustained release; Hyaluronic acid

29

30

31

32

33

34 Introduction

35 Rheumatoid arthritis (RA) is an autoimmune disease that is characterized by chronic synovial
36 inflammation. It affects about 1% of the adult all over the world and can cause serious damage of
37 cartilage and bone, and finally lead to disability [1]. Currently, RA is normally treated by oral
38 administration or injection of non-steroidal anti-inflammatory drugs (NSAIDs) or corticosteroids [2].
39 These strategies can decrease inflammation and retard the progression of RA by interfering with
40 inflammation related pathways, for example by decreasing the levels of pro-inflammatory cytokines,
41 inhibiting cell-mediated immune responses, or suppressing synovial collagenase gene expression [3, 4].
42 However, these traditional strategies suffer from low patient compliance due to the pain or infection
43 caused by the injection or the serious gastrointestinal side effects observed after frequent oral
44 administration. Additionally, the harsh gastrointestinal environment and liver first-pass effect could
45 result in a significantly low drug bioavailability [5].

46 As an attractive alternative, transdermal delivery systems for RA have been receiving increasing
47 attention [6]. Transdermal delivery of RA drugs could avoid gastrointestinal digestion in oral route and
48 pain sensation caused by injection. Furthermore, the easiness for self-administration further increases
49 their attractiveness. Small-molecule drugs formulated in transdermal patch or gel have been shown to
50 diffuse into the skin and exhibit anti-RA effect [7, 8]. However, the passive diffusion of drug is
51 significantly limited by the robust skin barrier, and has strict requirements on the properties of applied
52 drugs, including log p-value of 1-3, molecular weight below 500 Da and appropriate amount of H-bond
53 donors and acceptors [6]. Besides, penetration enhancers and nanoparticle technology have been
54 utilized to improve drug delivery efficiency through the skin [9-11]. Nevertheless, transdermal delivery
55 of biological drugs in a therapeutically relevant amount is still challenging due to their often large
56 molecular weight and high hydrophilicity [12].

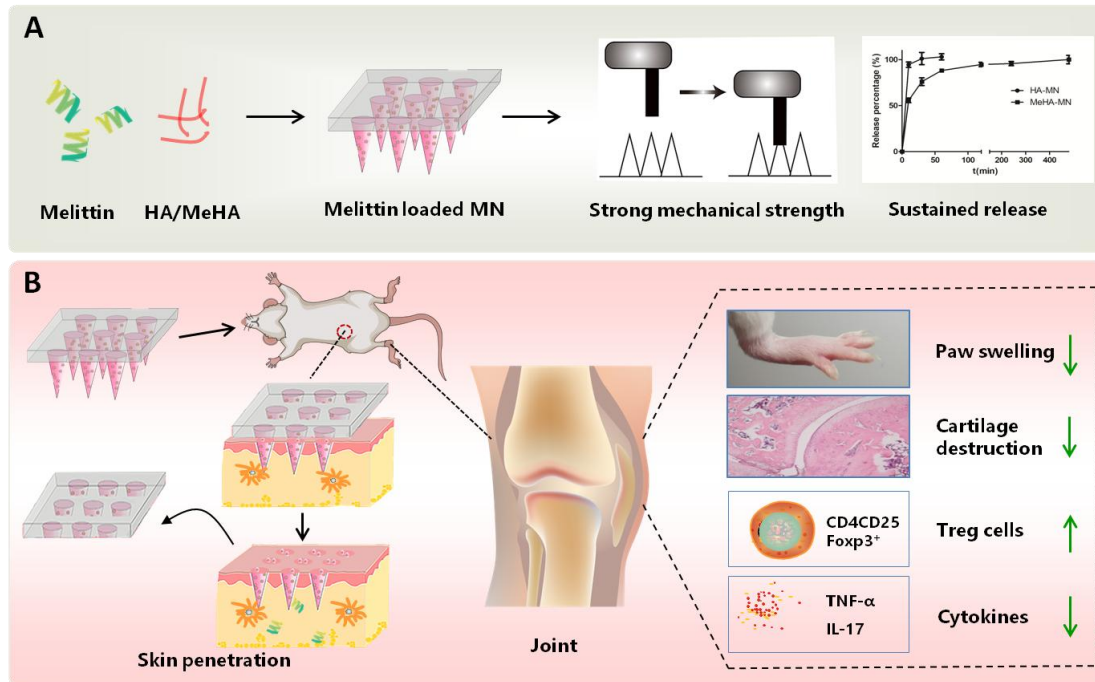
57 Polymeric microneedles are micro-structured needles with a length of 200-1000 μm . They can overcome
58 the skin barrier in a non-invasive and pain-free way as they are long enough to penetrate the skin but
59 short enough not to touch the nerves and blood vessels [13, 14]. Compared to traditional transdermal
60 gel or patch, microneedles can significantly increase transdermal delivery efficiency of biological drugs
61 such as protein and peptide drugs [15]. Additionally, polymeric microneedles do not result in any
62 hazardous waste after administration and the easiness for polymer functionalization allows possibilities
63 to modulate release properties of the loaded drugs. Hyaluronic acid (HA) is one of the mostly used
64 polymers for fabrication of polymeric microneedles and can dissolve within minutes after being inserted
65 into the skin. After modifying HA with functional groups, the obtained microneedles can be endowed
66 with controlled release properties of the loaded drugs, which have been shown to increase therapeutic
67 efficacy of the microneedles [16, 17].

68 As compared to metal or silicone microneedles, polymeric microneedles possess relatively much lower
69 mechanical strength, which may cause insufficient penetration of the skin and result in low drug delivery
70 efficiency [18, 19]. In previous studies, researchers have characterized the mechanical strength of
71 polymeric microneedles by compressing the whole patch with a flat surface and calculating the rupture
72 force of single microneedles by dividing the rupture force of the patch by the number of microneedles

73 [19, 20]. However, this method is not adequate since it can not give possible variations among the
74 microneedles within the patch, and the calculated mechanical property parameter is limited to rupture
75 force. In our lab, we have applied a micromanipulation technique to precisely characterize the
76 mechanical properties of individual microneedles. We have observed that as compared to rupture force,
77 rupture stress is a better indicator for the mechanical strength of the microneedles [21, 22].

78 Previous studies including several clinical trials conducted in East Asia have indicated that bee venom
79 acupuncture exerted anti-inflammation efficacy with minimum side effects in arthritis diseases [23].
80 Further studies revealed that the water-soluble fractions of bee venom can establish anti-inflammatory
81 effect and reduce disease progression in RA [24, 25]. It turned out that melittin, a cationic peptide
82 containing 26 nucleic acids, is the main component in bee venom for immune modulation and anti-RA
83 effects [26]. However, the use of live bees or injection of purified melittin could cause significant pain
84 and melittin itself has also a risk for causing serious hemolysis after intravenous injection [27]. These
85 drawbacks have significantly limited the therapeutic application of melittin for RA. Transdermal delivery
86 of melittin, for example by using microneedles, could potentially overcome the drawbacks mentioned
87 above. So far, to our best knowledge, there has been no report on the delivery of melittin by using
88 microneedles.

89 In the current study, we propose to develop melittin-loaded polymeric microneedles for the treatment
90 of RA, aiming for increasing patient compliance and therapeutic potency. The scheme is shown in Figure
91 1. Melittin was loaded into HA based microneedles and the mechanical strength of individual
92 microneedles was characterized by micromanipulation. The therapeutic potency of the fabricated
93 microneedles to treat RA was investigated in both rodent and murine AIA models. We showed that
94 although the loading of melittin decreased the mechanical strength of the microneedles, the drug
95 loaded in the microneedles was successfully delivered into the skin and significantly inhibited the
96 progression of RA by reducing excretion of pro-inflammatory cytokines and by altering cellular immunity.
97 We also observed that after modifying HA with methacrylate groups, the obtained microneedles with
98 sustained release properties could further increase therapeutic efficacy. Our study suggested that
99 polymeric microneedles for transdermal delivery of biological drugs could be a promising RA treatment
100 strategy for improving patient compliance and therapeutic potency.



101

102 **Figure 1.** Scheme of microneedle-mediated delivery of melittin for RA treatment. A: Fabrication of
 103 microneedles and characterization of mechanical strength and release behavior. B: The fabricated
 104 microneedles successfully delivered melittin into the skin and inhibited RA progression, as shown by
 105 results in histological, paw swelling, and levels of pro-inflammatory cytokines and Treg cells. HA:
 106 hyaluronic acid, MN: microneedles, MeHA: methacrylate modified hyaluronic acid, Treg: CD4 regulatory
 107 T cells.

108 **2 Materials and methods**

109 **2.1 Materials**

110 HA with a molecular weight of 10,000 Da was obtained from Bloomage Biotechnology (Jinan, China).
 111 Melittin ($\geq 96\%$) with an amino acid sequence of GIGAVLKVLTTGLPALISWIKRKRQQ-NH₂ was obtained
 112 from GL Biochem Ltd. (Shanghai, China). SYLGARD™ 184 silicone elastomer containing both base and
 113 curing agent was purchased from DOWSIL (MI, US). Fluorescein isothiocyanate (FITC) and Cy5 dye were
 114 purchased from Meilunbio (Dalian, China). Methacrylic anhydride (MA), N'-methylenebisacrylamide
 115 (MBA), Irgacure 2959 and NaOH were purchased from Sigma Aldrich (Shanghai, China). 4%
 116 paraformaldehyde was obtained from Leagene Biotechnology (Beijing, China). Anhydrous silica gel was
 117 purchased from Chron Chemicals (Chengdu, China). Antibodies for CD3, CD4, CD25, Foxp3, and Elisa kits
 118 for TNF- α and IL-17 were obtained from Invivogen (Toulouse, France). Optimal cutting temperature
 119 compound (OCT) medium was purchased from Sakura (Shanghai, China). Milli Q water (18 M Ω /cm,
 120 Millipore Co.) was used for the preparations of all solutions. All other reagents used were of analytical
 121 grade and used as received.

122 **2.2 Synthesis of methacrylate modified hyaluronic acid (MeHA)**

123 MeHA was synthesized by modifying HA with methacrylate groups as previously described [28]. Briefly,
124 5 g of HA was added into 100 mL water and incubated overnight for complete dissolution. 8 mL MA was
125 subsequently added into HA solution and pH of the solution was adjusted to 8. The mixture was then
126 stirred at 4 °C and incubated for overnight. Afterwards, the obtained MeHA was precipitated by acetone,
127 washed by ethanol for 3 times and dialyzed against water for 48 h to remove excess MA. Finally, the
128 purified MeHA was dried in an ice condenser (Labconco FreeZone 2.5, Hampton, VA) in freeze vacuum (-
129 50 °C, 90 mbar) overnight, and stored in dry environment for further use and analysis.

130 To verify if the chemical modification was successful, the ¹H nuclear magnetic resonance (¹H NMR)
131 spectrum of the obtained MeHA was characterized by using a Bruker 400 MHz NMR spectrometer
132 (Bruker, Switzerland) in CDCl₃.

133 2.3 Fabrication of melittin loaded microneedles

134 HA-based microneedles were fabricated by using a micro-molding method. Briefly, a stainless steel
135 microneedle patch, which contains 10×10 needles with a needle length of 700 μm and base to base
136 length of 300 μm on a plate of 0.9×0.9 cm², was first used to make polydimethylsiloxane (PDMS) mold.
137 The metal microneedle patch was immersed in SYLGARD™ 184 silicone elastomer containing base and
138 curing agent with a volume ratio of 10:1, and the mixed agent was cured by heating at 90 °C for 2 h.
139 Next, the metal microneedle patch was peeled off and the obtained PDMS mold was used for fabrication
140 of the microneedles.

141 To prepare melittin loaded HA microneedles (Mel-HA-MN), appropriate amount of melittin was first
142 dissolved into 1 mL of 500 mg/ml HA solution. Next, 30 μL of the matrix solution was filled into the
143 PDMS mold using pressurized air at 0.2 MPa for 3 min. After removing the excess matrix solution, the
144 matrix in the mold was dried in a glass dessicator containing anhydrous silica gel for 1 h. In the next step,
145 40 μL of HA solution (500 mg/mL) was added into the mold to prepare back-plate of the patch. The mold
146 was dried in the anhydrous silica gel environment for another 4 h. Finally, the microneedle patch was
147 peeled off from the PDMS mold and stored for further use and analysis. To fabricate melittin loaded
148 MeHA microneedles (Mel-MeHA-MN), 30 μL of polymer solution consisting appropriate amount of
149 melittin, 40 mg/mL MeHA, 20 mg/mL MBA and 0.5 mg/mL photo-initiator Irgacure 2959 was first filled
150 into the PDMS mold by pressurized air as mentioned above. The matrix in PDMS mold was dried in
151 anhydrous silica gel environment for 1 h, and 60 μL of blank HA solution (500 mg/mL) was further added
152 to fabricate the back-plate. The rest of the procedures were the same as that for fabrication of Mel-HA-
153 MN. Finally, the dried microneedle patch was cross-linked by ultraviolet radiation at 365 nm for 15 s.
154 The fabricated microneedle patches contain either 15 μg or 100 μg melittin per patch, which were used
155 for mice and rat study, respectively. To fabricate melittin-loaded microneedles for visualization by
156 confocal laser scanning microscopy (CLSM), FITC or Cy5 labelled melittin was used for the fabrication of
157 microneedles. To obtain FITC- or Cy5-labelled melittin, melittin was incubated with FITC or Cy5 dye for 1
158 h, and the excess free dye was removed using a dialysis bag with a cut-off of 2,000 Da.

159 2.4 Visualization of microneedles

160 Surface morphology of the fabricated microneedles was characterized by both scanning electronic
161 microscopy (SEM) and CLSM. For SEM visualization, the microneedles were coated with a thin layer of
162 carbon and visualized with a voltage of 15.0 KV by using a FEI Nova NanoSEM (Eindhoven, The
163 Netherlands). For visualization by CLSM, the microneedles were scanned with a step speed of 5 $\mu\text{m}/\text{step}$
164 by using a 10 \times Plan Apo objective.

165 2.5 Characterization of mechanical properties of individual microneedles

166 The mechanical properties including rupture behavior of individual microneedles were characterized by
167 using micromanipulation as previously reported [21]. Briefly, individual microneedles were put between
168 the sample stage of the micromanipulation instrument and an optical glass rod made of Borosilicate
169 with a diameter of 100 μm as a sensor of a force transducer (Model GSO-10, Transducer Techniques, LLC,
170 USA). Single microneedles were compressed between the stage and the glass probe with a compression
171 speed of 2 $\mu\text{m}/\text{s}$. The curve of compression force versus microneedle deformation was recorded. With
172 this information as well as mathematic modeling, rupture displacement and rupture stress of individual
173 microneedles were obtained, which has been described with details in a previous study [21]. The
174 compression process is shown in Supplementary video. For each type of patch, 30 microneedles were
175 analyzed.

176 2.6 In vitro release behaviors of HA-based microneedles

177 To study in vitro release behavior of the microneedles, each patch was suspended in 1 mL PBS and
178 shaken in a Bluepard shaker (Shanghai, China) with a speed of 100 rpm at 37 $^{\circ}\text{C}$. At different time points
179 (0, 10, 30, 60, 120, 240 and 480 min), 100 μL of the solution was withdrawn for analysis and the same
180 volume of fresh PBS was added back. The concentration of melittin in the release solution was analyzed
181 by a high-performance liquid chromatography (HPLC) (Agilent1260 Infinity, CA, USA) equipped with a
182 Diamonsil C18 column (Dikma, Beijing, China). The mobile phase includes 0.1% trifluoroacetic acid (TFA)
183 in water (solvent A) and 0.1% TFA in acetonitrile (solvent B). The composition of mobile phase changes
184 from 95% solvent A/5% solvent B to 5% solvent A/95% solvent B within 25 min. The absorbance was
185 detected at 220 nm. The concentration of melittin was calculated by using a calibration curve
186 ($y=2.5819x+2.6778$, $R^2=0.9998$).

187 2.7 Animals used in this study Male BALB/c mice of 6-8 weeks old (body weight 18-20 g) and male
188 Sprague Dawley (SD) rats of 6-8 weeks old (body weight 180-200 g) were purchased from Dashuo
189 Biotechnology Company (Chengdu, China). All animal experiments were performed following guidelines
190 approved by the ethics committee of Sichuan University. The animals were housed under standardized
191 conditions in the animal facility.

192 2.8 Penetration capacity of the fabricated microneedles in animal skin

193 The penetration capacity of fabricated microneedles was evaluated by Trypan blue staining method.
194 Briefly, the microneedles loaded with melittin were applied manually onto the skin. After 1 min, the
195 microneedle patch was removed and the penetrated skin was stained with 200 μL 4% Trypan blue for 2
196 min. After removing the excess dye and washing with water for 3 times, the stained skin was visualized

197 by bright field microscopy. To evaluate the penetration depth, microneedles loaded with FITC labeled
198 melittin were applied onto the skin. After 3 min, the back-plate of microneedles was removed and the
199 penetrated skin was excised, embedded in optimal cutting temperature compound (OCT) medium and
200 sectioned by using a Leica CM 1950 freezing microtome (Buffalo Grove, IL). Next, the inserted
201 microneedle tips in the skin specimens were visualized by a 10× Plan Apo objective.

202 2.9 In vivo release and biodistribution of melittin from Mel-MeHA-MN

203 The in vivo release behavior of melittin from Mel-MeHA-MN was evaluated in BALB/c mice skin. MeHA
204 microneedles loaded with Cy5 labelled melittin or free Cy5 were penetrated into mice abdomen skin as
205 described above. Afterwards, the fluorescence in the animal skin was visualized by using a PerkinElmer
206 in vivo imager (Shanghai, China) at different time points. The animals were monitored at day 1, 2, 3, 4, 6
207 and 7.

208 To investigate the biodistribution of melittin, Cy5-labelled melittin was given to BALB/c mice by either
209 S.C. injection or Mel-MeHA-MN. At 8 h after administration, the mice were sacrificed and tissues
210 including heart, liver, spleen, lung, kidney, joint and blood were isolated for visualization by the in vivo
211 imager. Blood containing 10 µg/ml melittin was used as a control.

212 2.10 Therapeutic potency of Mel-HA-MN in adjuvant-induced arthritis (AIA) rodent model

213 To build rat AIA model, SD rats were injected into each of hind foot pad with 80 µL complete Freund's
214 adjuvant which contains 10 mg/mL Mycobacterium tuberculosis on day 0. From day 4 when early
215 arthritis was established, the animals were treated by Mel-HA-MN loaded with 100 µg melittin or by
216 subcutaneous (S.C.) injection of the same dose on abdomen skin every other day for 8 times (n=6). The
217 doses were selected by referring to previous studies [29, 30]. AIA rats without any treatment were used
218 as a control. On day 22, the animals were sacrificed and paws and blood were collected for further
219 analysis.

220 During the treatment, the weight of animals was recorded to calculate the percentage of the weight loss
221 compared to the base. The thickness of two hind paws was measured using a vernier caliper every other
222 day to calculate the average change of ankle thickness. The clinical symptoms were scored at a scale of
223 0-4 (0, no erythema or swelling; 1, mild erythema and swelling confined to ankle joint; 2, mild erythema
224 and swelling extending from the ankle to the tarsals; 3, moderate erythema and swelling extending to
225 metatarsal joints; 4, pronounced erythema and swelling of entire paw).

226 The blood on day 22 was withdrawn to study the hematologic parameters including counts of white
227 blood cells (WBC), red blood cells (RBC) and platelets. Analysis was performed on a Mindray BC-2800 Vet
228 (Shenzhen, China).

229 For histological examination, the collected paws were first fixed in 4% paraformaldehyde for 24 h. The
230 fixed paws were immersed in saturated EDTA-2Na solution and shaken in a Bluepard shaker (Shanghai,
231 China) with a speed of 180 rpm for 2 month for decalcification of the paws. The saturated EDTA-2Na
232 solution was refreshed every week until the decalcification was complete. Next, the paws were

233 embedded in paraffin, sectioned at 5 μm and stained with haematoxylin and eosin (H&E) or Safranin O-
234 fast green. The inflammatory cell influx and cartilage integrity were assessed.

235 2.11 Therapeutic potency of Mel-MeHA-MN in murine AIA model

236 Mouse AIA model was induced by injection of 20 μL complete Freund's adjuvant which contains 10
237 mg/mL Mycobacterium tuberculosis into each of the hind foot on day 0. Starting from day 4, when the
238 early arthritis was established, male BALB/c mice of 6-8 weeks old were treated with the following
239 groups: 15 μg melittin loaded Mel-MeHA-MN, 15 μg melittin loaded Mel-HA-MN and S.C. injection of 15
240 μg melittin. AIA mice receiving no treatment were used as a control. The various formulations were
241 administered every other day for 6 times. On day 16, mice were sacrificed and blood, hind paws, spleen
242 and popliteal lymph nodes were collected for further analysis. The animal weight loss, hind paw
243 thickness change and arthritic scores were monitored using the same method as described for the
244 therapeutic potency study in AIA rodent model.

245 Pro-inflammation cytokines including TNF- α and IL-17 in the serum and paws were measured using
246 ELISA kits according to the manufacturer's instructions. Serum was obtained by centrifuging the
247 collected blood at 2000 g for 10 min with a Sigma 3K15 (Shanghai, China). The collected paws were cut
248 into small pieces, suspended in PBS to reach a mass concentration of 1 g/mL and processed with glass
249 homogenizers. The obtained suspension was centrifuged at 2500 g for 10 min to obtain the supernatant.
250 To measure the cytokine concentrations, 100 μL of capture antibody in coating buffer was added into
251 each well of 96 well-plates and incubated at 4 $^{\circ}\text{C}$ for overnight. After washing the wells with 300 μL
252 buffer for 3 times, 200 μL of block buffer was added into each well and incubated for 1 h at room
253 temperature. The plates were washed and 100 μL of standards or samples was added into each well and
254 incubated for another 2 h at 4 $^{\circ}\text{C}$. Next, 100 μL of detecting antibody was added into each well and
255 incubated at room temperature for 1 h. The plates were washed again for 4 times and 100 μL of diluted
256 Horseradish peroxidase conjugate (HRP) was added into each well and incubated for 30 min at room
257 temperature. Subsequently, 100 μL of tetramethylbenzidine (TMB) solution was added into each well
258 and incubated for 15 min. Finally, the reaction was stopped by adding 150 μL of 2 M sulfuric acid and
259 the absorbance was measured at 450 nm with a Tecan Spark 10M plate reader (Männedorf,
260 Switzerland).

261 The blood on day 16 was withdrawn to study the hematologic parameters as described in the last
262 section, including WBC, RBC, platelets and percentage of lymphocytes, monocytes and granulocytes in
263 WBC. H&E stain analysis was performed according to the same procedure as described in the
264 therapeutic potency study of AIA mouse model.

265 Percentage of CD4 T regulatory cells (Treg) in spleen and popliteal lymph nodes were measured by flow
266 cytometry (Cytomics FC 500, Beckman, Indianapolis, IN, USA). Briefly, single cell suspensions were
267 obtained by forcing the spleen and popliteal lymph node through 70 μm strainers. The cells were
268 centrifuged at 500 g for 5 min and washed with PBS for two times. Subsequently, the cells were
269 resuspended in PBS and 200 μL of the cells was transferred to each well of 96-well plates. 100 μL of
270 diluted surface staining antibodies including APC conjugated anti-CD3, APC-Cy7 conjugated CD4 and FITC

271 conjugated CD25 were added into each well and incubated for 30 min in the dark at 4 °C. After washing
272 with FACs buffer, the cells were resuspended in freshly prepared fixation/permeabilization solution and
273 incubated for 30 min at 4 °C. The cells were then washed with the permeabilization buffer and
274 resuspended in diluted PE-conjugated anti-Foxp3 antibody solution for 30 min. Finally, the cells were
275 washed with permeabilization buffer and the percentage of Treg cells (CD3CD4CD25Foxp3⁺) was
276 analyzed by the flow cytometry. The data were analyzed by using a FlowJo software.

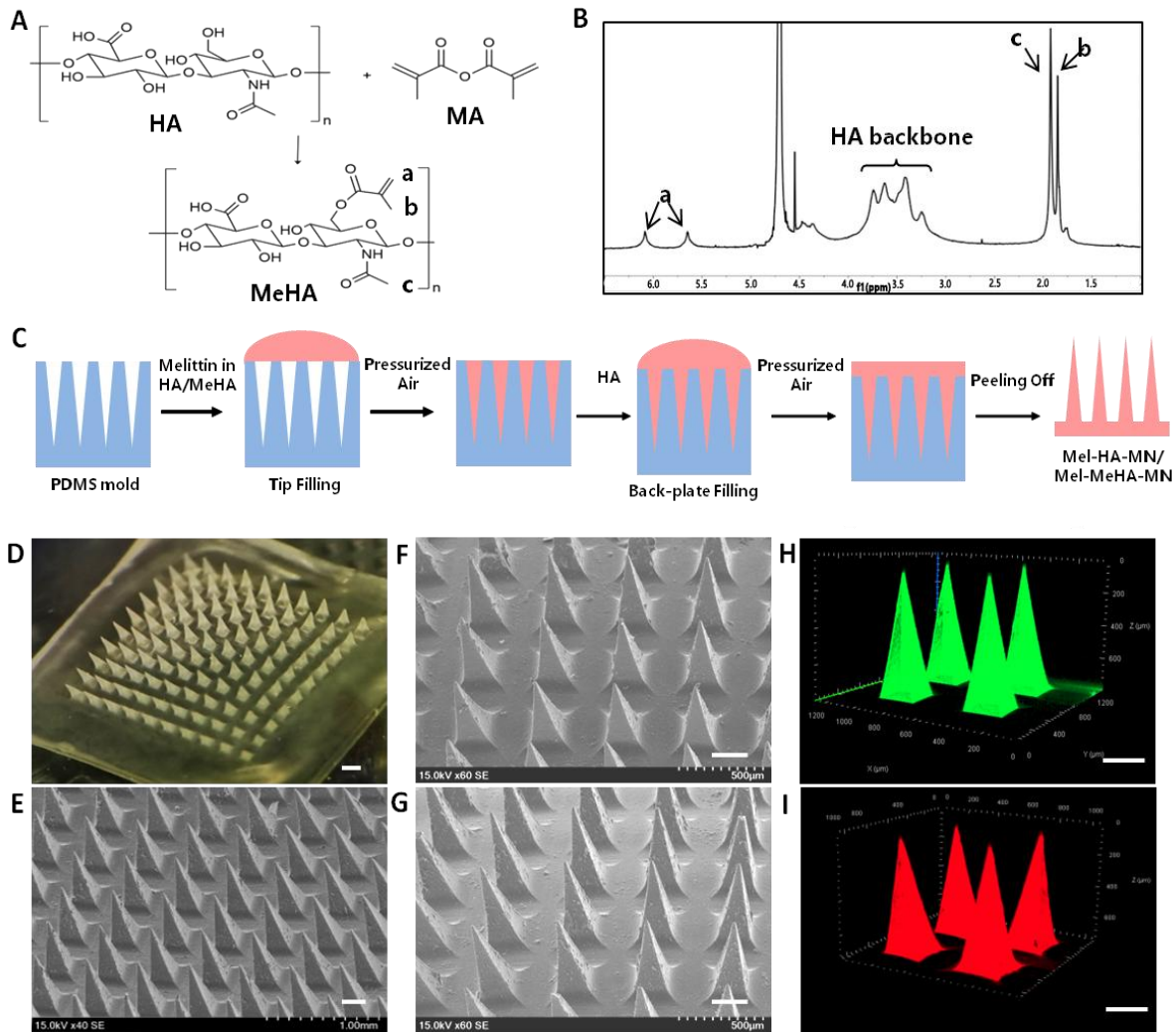
277 2.12 Statistical analysis

278 All the data of immunization studies were analyzed by one way ANOVA with Turkey post-test by using
279 GraphPad Prism (version 5.02). The significant levels were set at *p<0.05, **p<0.01 and ***p<0.001.

280 3. Results

281 Fabrication of Mel-HA-MN and Mel-MeHA-HA

282 MeHA was obtained by modifying HA with methacrylate groups as shown in Figure 2a. The successful
283 modification was indicated by ¹H NMR spectrum peaks at 5.6 ppm (a, 1H, CH¹H=C(CH₃)CO), 6.1 ppm (a,
284 1H, CHH¹=C(CH₃)CO), 1.85 ppm (b, 3H, CH₂=C(CH₃)CO) and 1.92 ppm (c, 3H, NHCOCH₃) (Figure 2B). Our
285 results showed that the yield was around 80% and the modification degree was around 32% by
286 comparing the area of peaks under 5.6 and 6.1 ppm to the peak area under 1.92 ppm. Mel-HA-MN and
287 Mel-MeHA-MN were fabricated by using micro-molding with a process as shown in Figure 2C. The
288 microneedle patches were fabricated by a two-step filling method to avoid waste of drug. Bright field
289 and SEM Images of microneedles (Figure 2D-2G) showed that the fabricated microneedles had a regular
290 rectangular pyramid shape with sharp tips. As compared to the blank HA microneedles (Figure 2D-2E),
291 the loading of melittin did not significantly change the tip sharpness or surface morphology of the
292 corresponding microneedles (Figure 2F-2G). CLSM images of HA microneedles loaded with FITC labeled
293 melittin (Figure 2H) and MeHA microneedles loaded with Cy5 labelled melittin (Figure 2I) indicated that
294 melittin was uniformly distributed in the microneedles. The surface morphology of microneedles shown
295 by CLSM was consistent with that of SEM, further confirming that we have successfully fabricated
296 melittin loaded HA and MeHA microneedles.



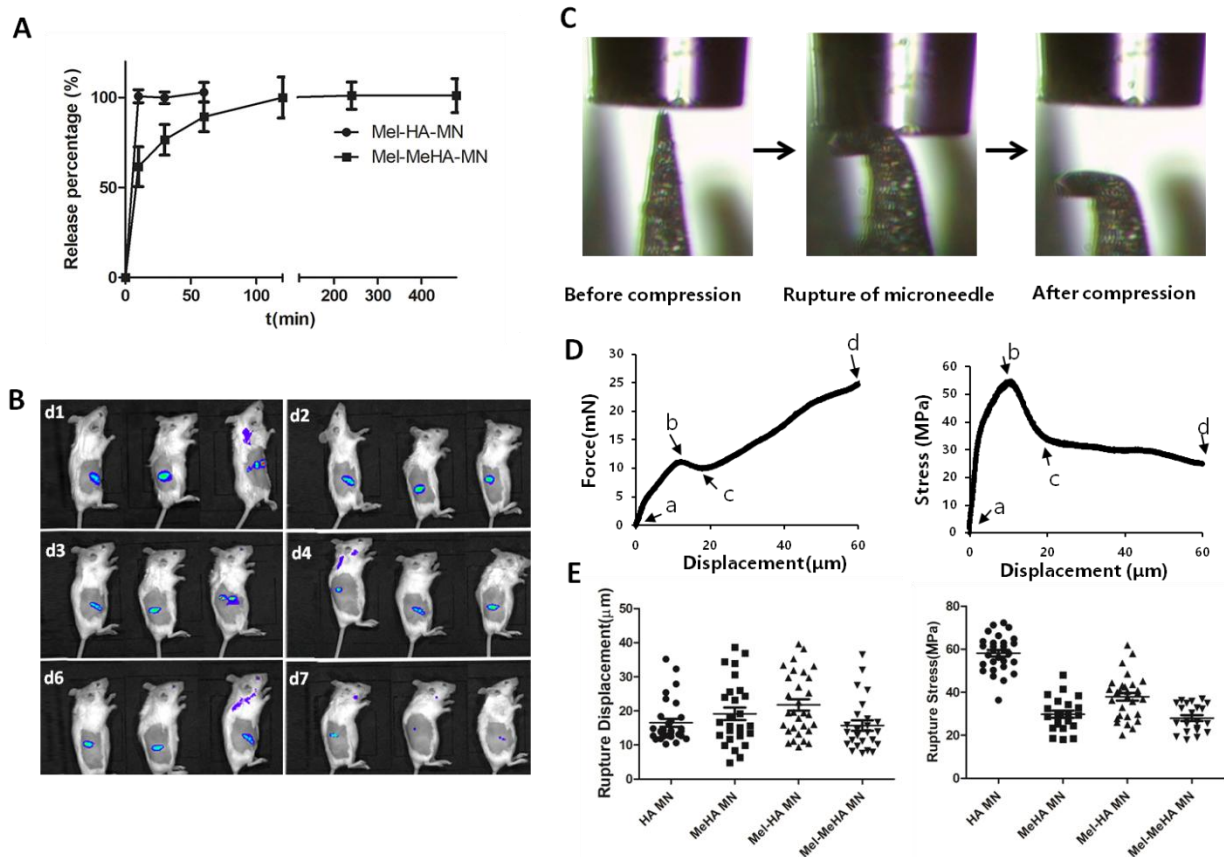
297
 298 **Figure 2.** Fabrication and characterization of Mel-HA-MN and Mel-MeHA-MN. A: Synthesis of MeHA by
 299 modifying methacrylate groups on HA molecules. B: ^1H NMR spectrum of MeHA indicated the successful
 300 modification of methacrylate groups on HA. C: Scheme of micro-molding method for fabrication of
 301 microneedles. D: Bright field image of blank microneedles. E-G: Scanning electronic microscopy (SEM)
 302 images of blank microneedles (E), Mel-HA-MN (F) and Mel-MeHA-MN (G). H: Confocal laser scanning
 303 microscopy (CLSM) image of HA microneedles loaded with FITC labelled melittin. I: CLSM image of MeHA
 304 microneedles loaded with Cy5 labelled melittin. Scale bar: 200 μm .

305 Characterization of release behavior and biodistribution of melittin

306 Next, we investigated and compared *in vitro* release behaviors of Mel-HA-MN and Mel-MeHA-HA in PBS.
 307 As shown in Figure 3A, all melittin was released from HA microneedles within 10 min. By contrast, Mel-
 308 MeHA-MN showed a burst release percentage of 56 % within 10 min and the rest of protein was
 309 sustainedly released until 480 min. The *in vivo* sustained release behavior of Mel-MeHA-MN was also
 310 evaluated in mice skin by using *in vivo* imager. Mel-MeHA-MN loaded with Cy5 labelled melittin was
 311 applied onto abdomen skin of BALB/c mice and the fluorescence of melittin was monitored on day 0, 2,
 312 3, 4, 6 and 7. It was shown that the inserted microneedles remained in the skin and sustainedly released

313 melittin for 7 days, as shown by the slow elimination of fluorescence of melittin (Figure 3B). By contrast,
314 the free Cy5 was eliminated within 3 days (Supplementary Figure 1).

315 The biodistribution of melittin was investigated by in vivo imager. As shown in Supplementary Figure 2,
316 melittin was observed in liver, lung, kidney, joints and blood after both S.C. and microneedle application.
317 Additionally, melittin level in the blood of the two treatment groups was much lower than the hemolytic
318 concentration, as indicated by the much lower fluorescence intensity.



319 **Figure 3.** Release behavior and mechanical properties of the fabricated microneedles. A. In vitro release
320 behaviors of Mel-HA-MN and Mel-MeHA-MN. B. In vivo release of Mel-MeHA-MN in BALB/c mice. C.
321 Different status of single microneedles during compression by micromanipulation. D: Typical curves of
322 rupture force and rupture stress versus microneedle displacement during compression. E: Rupture
323 displacement and rupture stress of different microneedle patches.
324

325 Characterization of mechanical strength of the fabricated microneedles

326 Next, we evaluated the mechanical strength of individual microneedles by using micromanipulation. In
327 Figure 3C, different status of microneedles during compression were shown, which are also reflected in
328 Figure 3D. The microneedles were compressed at point a, and ruptured at point b where both rupture
329 force and rupture stress increased to a peak. The rupture force decreased to point c and increased again
330 until the end of the compression (point d). Instead, the rupture stress decreased to point c and showed a
331 slower decrease until point d. With this information as well as mathematic modeling [21], the rupture

332 displacement and rupture stress were obtained. As shown in Figure 3E, all microneedles ruptured at a
333 displacement of around 10-20 μm . The loading of melittin significantly decreased the mechanical
334 strength of the microneedles: melittin loading decreased the rupture stress of HA microneedles from 58
335 MPa to 38 MPa, while the loading into MeHA microneedles slightly decreased the rupture stress from 30
336 MPa to 27 MPa.

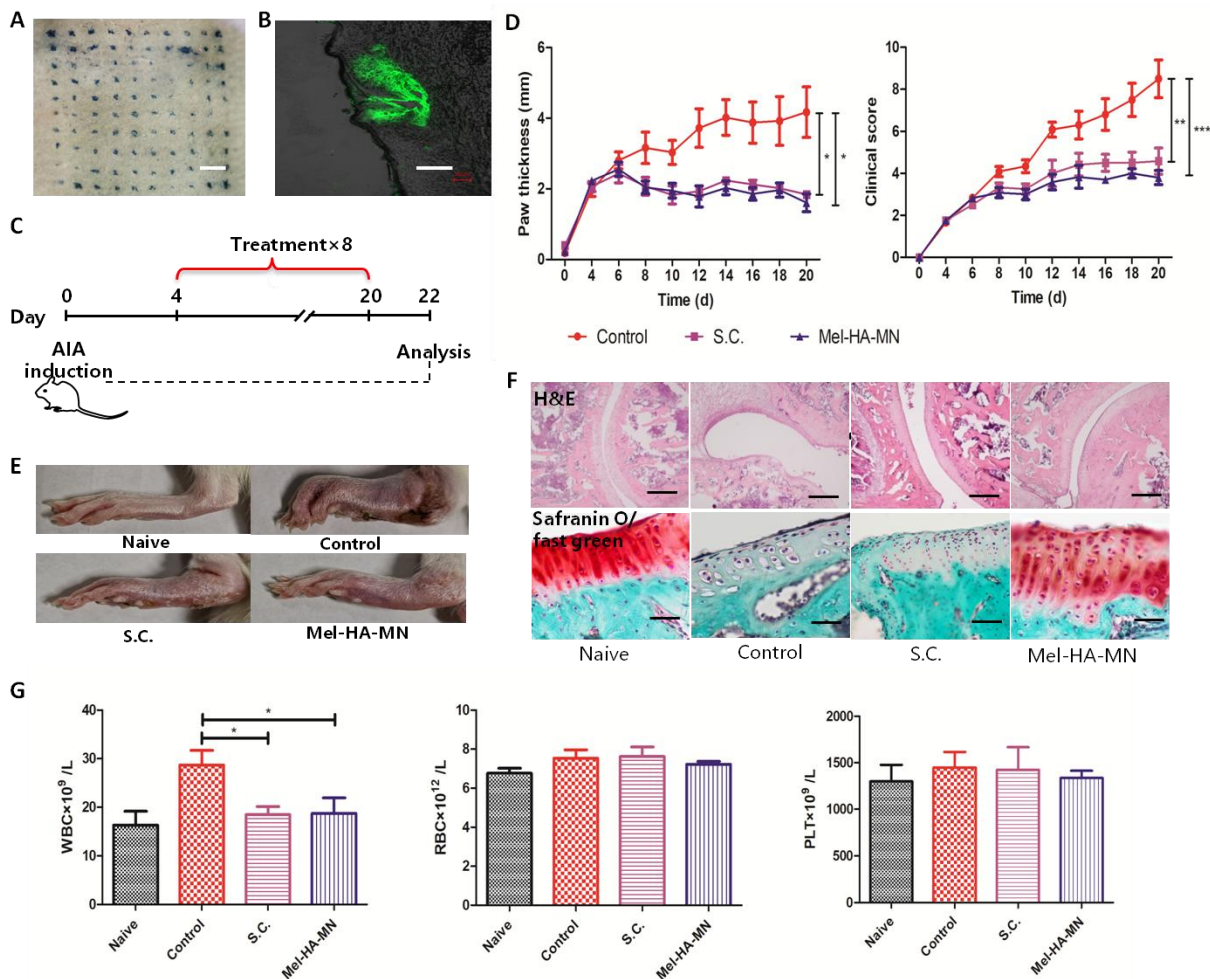
337 **Mel-HA-MN suppressed RA progression in AIA rodent model**

338 We first studied the therapeutic potency of Mel-HA-MN in the rat AIA model. To investigate the
339 penetration capacity of the microneedles, we applied the patch on the abdomen skin of rat, and the
340 penetration efficiency was investigated with Trypan blue staining method. It was shown that the
341 microneedles efficiently penetrated the skin (Figure 4A). To study the penetration depth of the
342 microneedles, the holes made by the microneedles in the sectioned specimens of the penetrated skin
343 were visualized by fluorescence microscopy. It was shown that Mel-HA-MN successfully pierced the skin
344 with a penetration depth of around 200 μm . Additionally, melittin was successfully released inside the
345 micro-holes made by microneedles after penetrating the skin for 3 min (Figure 4B).

346 Four days after induction of AIA, the microneedle patch was applied onto the animals every other day
347 for 8 times and the therapeutic potency was evaluated by monitoring the body weight loss, change of
348 paw thickness and clinical score of the symptoms (Figure 4C). As shown in Supplementary Figure 3,
349 animals in all groups showed a similar weight loss percentage as compared to the base (Naive rats).
350 Specifically, the weight loss percentage reached around 15% and stayed relatively stable until the end of
351 the experiment. The paw thickness of model control rats increased by above 4 mm at the end of
352 treatment (Figure 4D). By contrast, the paw thickness change of animals after receiving either S.C.
353 injected melittin or Mel-HA-MN increased to around 2.5 mm on day 6, but started to decrease gradually
354 to below 2 mm at the end of treatment, which was less than 50% of the thickness of model group.
355 Similarly, melittin treatment by both S.C. and Mel-HA-MN groups decreased the clinical score by two-
356 fold as compared to that in model control group (Figure 4D). The representative paw images further
357 confirmed that the administration of melittin significantly stabilized the swelling of the paw and
358 suppressed RA progression (Figure 4E).

359 Next, we checked the histology of the paws by H&E and Safranin O/fast green staining. The examination
360 by H&E stain showed that the treatment of Mel-HA-MN or S.C. injection of melittin significantly
361 preserved cartilage integrity and reduced the infiltration of leukocytes as compared to control group (a:
362 cartilage destruction, b: leukocyte infiltration, indicated by arrows, Figure 4F). Safranin O/fast green
363 staining showed similar trends as H&E staining that Mel-HA-MN and S.C. administered melittin
364 effectively preserved the integrity of the cartilage, as indicated by the red stain of the chondrocytes.
365 Hematologic parameters on day 22 were checked to examine the in vivo safety of our formulations.
366 Results showed that control group significantly increased the WBC level as compared to naive rats
367 (Figure 4G), probably due to the infection of *Mycobacterium tuberculosis* used for building the disease
368 model [31]. Interestingly, S.C. injected and Mel-HA-MN mediated delivery of melittin reversed this trend.
369 On the other hand, the treatment did not cause significant changes of RBC and PLT as compared to

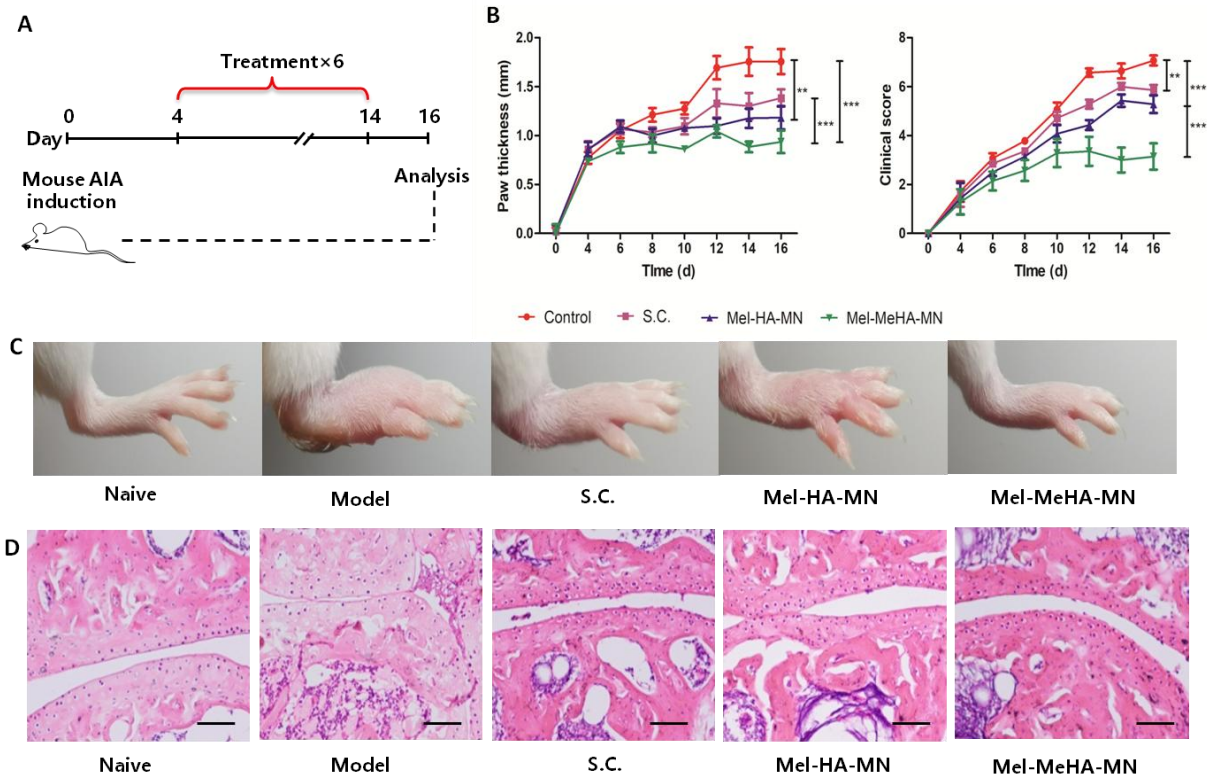
370 naive animals. To sum, Mel-HA-MN effectively delivered melittin into rat skin and inhibited RA
 371 progression in AIA rodent model.



372
 373 **Figure 4.** Therapeutic potency of Mel-HA-MN in rat AIA model. A: Penetrated skin stained by Trypan
 374 blue. Scale bar: 0.5 cm. B: Micro-channels made by Mel-HA-MN visualized by fluorescence microscopy.
 375 Scale bar: 100 μ m. C: Experimental strategy for therapeutic potency study of the microneedle patch. D:
 376 Change of paw thickness and clinical score during treatment. E: Representative paw images of different
 377 treatment groups. F: H&E and Safranin O/fast green stain images of paws. a: cartilage destruction, b: cell
 378 infiltration. Scale bar: 1000 μ m (upper) and 250 μ m (lower). G: Hematologic parameters on day 22
 379 including WBC, RBC and Platelets. Bars represent mean \pm SEM, n = 6. *p<0.05, **p<0.01 and ***p<0.001.

380 Mel-MeHA-MN significantly increased therapeutic efficacy in mouse AIA model

381 Next, we investigated and compared therapeutic potency of Mel-MeHA-MN to Mel-HA-MN in AIA
 382 mouse model. Mice were administered with either Mel-HA-MN or Mel-MeHA-MN. The mice were
 383 treated every other day for 6 times with a melittin dose of 15 μ g (Figure 5A).



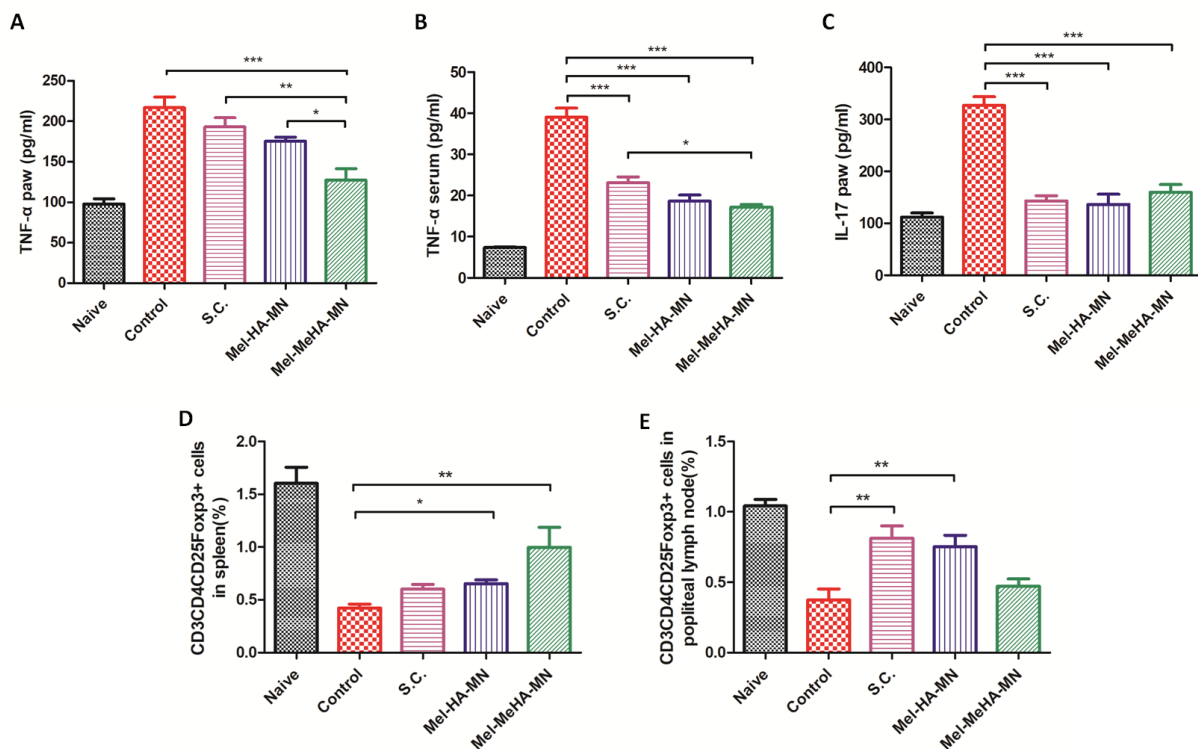
384
 385 **Figure 5.** Therapeutic potency of Mel-MeHA-MN in mouse AIA model. A: Schematic diagram for studying
 386 therapeutic efficacy of Mel-MeHA-MN. B: Paw thickness change and clinical score during treatment. C:
 387 Representative images of paws from different groups. D: H&E staining of mice paws. Scale bar: 400 μ m.
 388 Bars represent mean \pm SEM, n = 6. *p<0.05, **p<0.01 and ***p<0.001.

389 The therapeutic potency of our fabricated microneedle systems in mice AIA was evaluated by
 390 monitoring weight loss, paw thickness change and clinical score. As shown in Supplementary Figure 4,
 391 the administration of melittin seemed to decrease weight loss percentage although the difference
 392 between the treated groups and control group was not significant. By the end of the study, the animals
 393 showed a weight loss percentage of 10-15% as compared to the base. As for paw thickness change,
 394 subcutaneous injection of melittin and Mel-HA-MN decreased the paw thickness by 20% and 30%,
 395 respectively, as compared to model control (Figure 5B). Importantly, Mel-MeHA-MN group reduced the
 396 paw thickness by a significantly larger level to 50%. The results of clinical score showed a similar trend:
 397 Mel-MeHA-MN group significantly decreased the clinical score as compared to model and S.C. groups
 398 (**p<0.001, Figure 5B).

399 Representative paw images further confirmed that the treatment by melittin effectively reduced the
 400 symptoms of the RA, including paw swelling and erythema (Figure 5C). Mel-MeHA-MN with a sustained
 401 release property of melittin showed a better protection efficacy as compared to S.C. group and Mel-HA-
 402 MN. H&E staining indicated that microneedle delivered melittin significantly reduced the infiltration of
 403 inflammatory cells and preserved the integrity of cartilages (Figure 5D). To sum, these results shown
 404 above indicated that the administration of sustained release microneedles could further improve RA
 405 therapeutic efficacy of melittin as compared to HA microneedles and S.C. injected melittin.

406 **Melittin loaded microneedles reduced levels of pro-inflammation cytokines and increased Treg cell**
 407 **percentages**

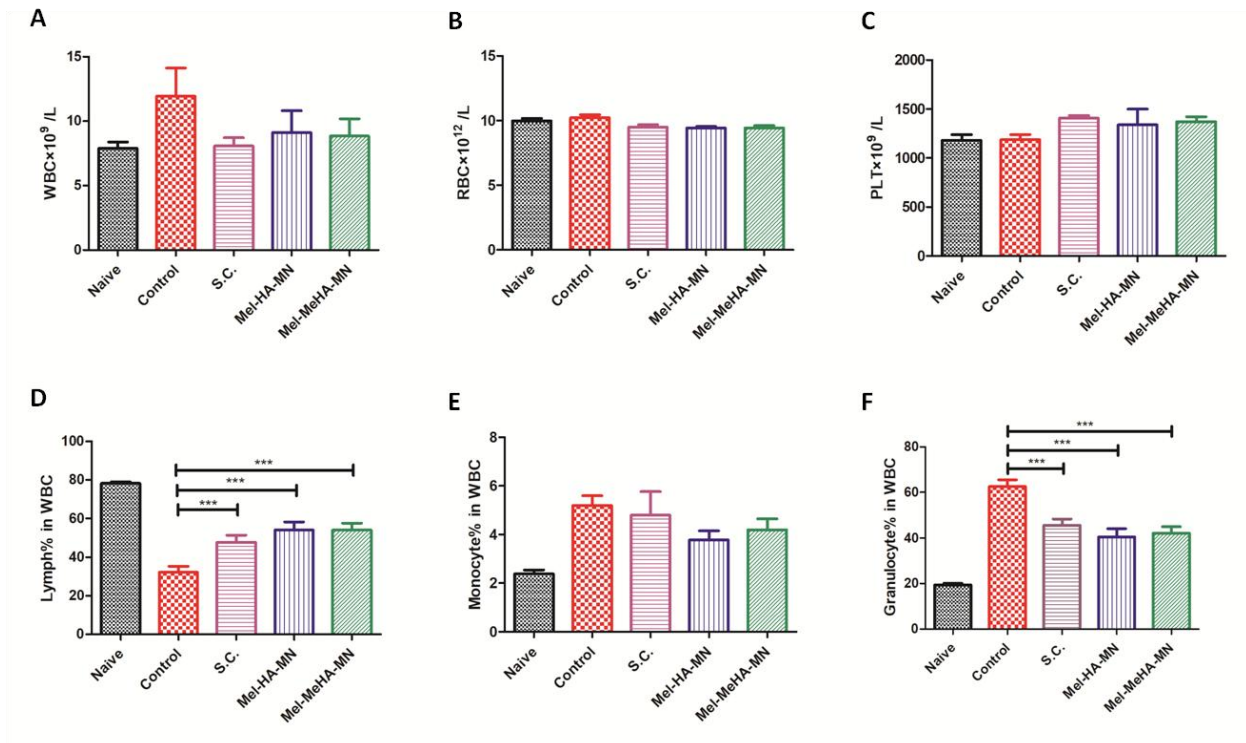
408 Next, we checked cytokine levels in the paws and blood serum to see if the application of melittin
 409 loaded microneedles inhibited RA progression by inhibiting expression of the pro-inflammation
 410 cytokines. We showed that TNF- α and IL-17 in both paws and serum were significantly decreased after
 411 the administration of melittin-loaded microneedles as compared to model control (Figure 6A-C).
 412 Specifically, Mel-MeHA-MN significantly decreased TNF- α levels in paws as compared to model control
 413 (** $p < 0.001$, Figure 6A). Importantly, Mel-MeHA-MN also induced significantly lower level of TNF- α
 414 than both S.C. group and Mel-HA-MN group (* $p < 0.05$). This trend was even more obvious for TNF- α in
 415 blood serum: microneedle-mediated delivery of melittin decreased TNF- α level by more than two times
 416 (Figure 6B). Mel-MeHA-MN showed a significantly stronger inhibition effect for TNF- α excretion than S.C.
 417 group. On the other hand, all groups after receiving melittin treatment significantly inhibited the level of
 418 IL-17 in paws by almost 3 times as compared to model control group. In this case, the difference
 419 between sustained release microneedle group and fast release microneedle and S.C. groups was not
 420 significant (Figure 6C).



421 **Figure 6.** Cytokines and Treg cell percentages on day 16. A: Concentration of TNF- α in paws of mice. B:
 422 Concentration of TNF- α in blood serum. C: Concentration of IL-17 in paws. D: Percentage of Treg cells in
 423 spleen. E: Percentage of Treg cells in popliteal lymph node. Bars represent mean \pm SEM, n = 6. * $p < 0.05$,
 424 ** $p < 0.01$ and *** $p < 0.001$.
 425

426 We next checked Treg cell percentages in spleen and popliteal lymph nodes on day 16 by analyzing the
 427 percentage of CD3CD4CD25Foxp3⁺ cells using flow cytometry. We observed that melittin delivered by

428 using microneedles significantly increased Treg cell percentage in spleen (Figure 6D). Additionally, the
 429 sustained release microneedle induced the highest level of Treg cells. As for Treg cells in popliteal lymph
 430 nodes, S.C. and HA-MN delivered melittin significantly increased the percentage of Treg cells as
 431 compared to model group (Figure 6E). Interestingly, the sustained release microneedle did not show any
 432 promotion of Treg cells in lymph nodes. These results above indicated that the microneedles may inhibit
 433 RA progression by inhibiting pro-inflammatory excretion and by increasing Treg cell percentages in
 434 lymphatic organs.



435 **Figure 7.** Hematologic parameters of microneedle-treated mice on day 16. A: White blood cell counts
 436 (WBC). B: Red blood cell counts (RBC). C: Platelets counts (PLT). D: Percentage of lymphocytes in WBC. E:
 437 Percentage of monocytes in WBC. F: Percentage of granulocytes in WBC. Bars represent mean ± SEM, n
 438 = 6. *p<0.05, **p<0.01 and ***p<0.001.

440 Finally, the hematologic parameters were checked to see if the treatment of melittin induced any blood
 441 cytotoxicity. Similar to the observation in rat AIA model, WBC counts were significantly increased in
 442 model control group, probably because of bacterial infection when building the RA disease model
 443 (Figure 7A). The use of melittin seemed to tune back this trend, although the difference between
 444 melittin treated groups and control group was not significant. The treatment by microneedles did not
 445 induce any significant change of RBC or PLT counts compared to naive mice (Figure 7B-C). Interestingly,
 446 control group showed significantly decreased percentage of lymphocytes, and increased percentages of
 447 monocytes and granulocytes as compared to naive cells, while the treatment by melittin loaded in
 448 microneedles effectively reversed this trend (Figure 7D-F).

449 **Discussion and conclusions**

450 Transdermal drug delivery systems for RA therapy are attractive as they could overcome several
451 drawbacks which exist in traditional strategies of oral uptake or injection of RA drugs, including low
452 compliance, infection risk and low drug bioavailability. However, transdermal delivery efficiency of RA
453 drugs especially for biological drugs is significantly limited due to the barrier function of stratum
454 corneum in the skin. In this study, we fabricated HA-based polymeric microneedles for transdermal
455 delivery of a peptide drug melittin, which is the main component for immune modulation and anti-RA
456 effect in bee venom, aiming for increasing administration convenience and skin delivery efficiency. Our
457 results showed that HA based microneedles could successfully overcome the skin barrier and deliver
458 melittin into the skin. The delivered melittin was able to effectively inhibit the progression of RA and
459 protect cartilage from being damaged, which was as effective as that induced by S.C. injection of
460 melittin. More importantly, by simply modifying HA with cross-linkable groups, the fabricated
461 microneedles could further increase the therapeutic efficacy. Our results revealed that microneedle
462 based delivery system could provide an attractive transdermal RA therapy with improved patient
463 compliance and therapeutic efficacy.

464 In this study, we first characterized the mechanical properties of individual polymeric microneedles by
465 micromanipulation technique. The micromanipulation instrument was initially used to characterize the
466 mechanical properties of individual cell and microparticles. In our previous study, we have extended its
467 use for characterization of individual polymer microneedles and shown that the micromanipulation
468 instrument is a very powerful tool for characterizing the mechanical properties of individual
469 microneedles. We have also shown that rupture stress is a better indicator for mechanical properties of
470 microneedles as compared to rupture force, as rupture stress can be regarded as an intrinsic material
471 property parameter of microneedles [21]. In the current study, we found that the loading of drug could
472 significantly decrease the rupture stress of the corresponding microneedles, which is similar to what we
473 observed in the last study. The mean ultimate rupture strength of human skin was reported to be $27.2 \pm$
474 9.3 MPa [32]. All the mean values of the obtained rupture stress of the microneedle patches in this work
475 are not less than this value, indicating that these microneedles may be strong enough to pierce the
476 human skin and our microneedles could have potential for future clinical use. Nevertheless, we showed
477 that our fabricated microneedles were strong enough to pierce and to deliver the loaded melittin into
478 the skin.

479 Traditional polymer based dissolving microneedles normally have a fast drug-dissolving rate after being
480 inserted into the skin [33, 34]. Recent research put a lot of efforts on developing microneedles with
481 controlled release properties of the loaded drugs, aiming for improving drug efficacy and reducing side
482 effects [14, 35]. We here fabricated melittin-loaded HA microneedles with slow-release properties by
483 simply modifying the polymer with cross-linkable groups. Our results showed that as compared to Mel-
484 HA-MN with fast release properties, the prepared Mel-MeHA-MN possessed improved therapeutic
485 capacity on inhibiting RA symptoms. Cytokine and cell immunity study revealed that the sustained
486 release microneedles could further decrease the levels of pro-inflammatory cytokines and increase the
487 Treg cell percentages. The observed advantages of sustained release microneedles were consistent with
488 previous findings that sustained release of drug or vaccine from microneedles could increase drug
489 efficacy or vaccine immunogenicity [17, 36-38]. For example, Gu et al. showed that MeHA based

490 microneedles could sustainedly release the loaded insulin, and as a result could better control blood
491 glucose level and improve the safety of insulin delivery [28, 39]. In another study, chitosan microneedles
492 loaded with a model antigen OVA elicited superior immune responses which lasted for more than 6
493 weeks after only one dose [40]. The improved therapeutic efficacy against RA by sustained release of
494 drug found in the current study is also consistent with our findings in previous research. For instance, we
495 have previously shown that after intravenous injection of polymeric micelles with sustained release
496 property of dexamethasone, the drug accumulation in the inflammatory joint was significantly increased
497 and their inhibition potency of RA was robustly enhanced [41-43]. In summary, our current study
498 indicates that microneedle based delivery system could be an alternative strategy for sustained delivery
499 of RA drug to improve RA drug efficacy.

500 Herein, we chose a peptide drug melittin to investigate the delivery capacity of our fabricate
501 microneedles. Previous studies have shown that melittin could inhibit RA progression by inhibiting the
502 excretion of pro-inflammatory cytokines after interacting with NF-KB pathway [44]. In our current study,
503 we indeed showed that microneedle-mediated delivery of melittin could inhibit expression of TNF- α and
504 IL-17 in both paws and blood serum. Additionally, we observed that the application of melittin could
505 increase Treg cell amount in lymphatic organs including spleen and popliteal lymph nodes. RA is an
506 autoimmune disease caused by the loss of self-tolerance while regulatory CD4⁺ T cells play a key role in
507 maintaining self-tolerance [45]. Although the mechanism of melittin to increase Treg cell amount
508 remains to be explored, our results indicated that microneedle-mediated delivery of melittin could have
509 potential for tuning of T cell imbalances in autoimmune diseases [46, 47].

510 Bee venom acupuncture has been used for the treatment of RA for a long time [48, 49]. However, the
511 significant pain sensation and requirement on live bees have significantly limited the application of this
512 strategy. Our results showed that microneedle-mediated melittin delivery could have potential to
513 improve this method. Specifically, microneedle strategies have advantages including easiness for
514 administration and potential for improving the stability of the loaded drug. Polymeric microneedles also
515 allow controlled drug release to improve drug therapeutic efficacy by polymer modification. Additionally,
516 although melittin has a risk to cause hemolysis due to their strong cell membrane penetrating function
517 [27, 50, 51], our results showed that the administration of melittin did not cause significant blood
518 cytotoxicity. Biodistribution results indicated that this could be caused by the fact that the blood
519 concentration of melittin was much lower than its hemolytic concentration (Supplementary Figure 2).

520 Finally, the relative low drug loading capacity of microneedles is one important factor limiting their
521 possible clinical translation. The amplification of loaded drug amount from the level for experiment
522 animal models to human is still a challenge lying in front before microneedles can be applied to patients.
523 In our current study, we investigated the therapeutic efficacy of sustained release microneedles in mice
524 model, partly due to the fact that our fabricated microneedles could easily fulfill sustainedly releasing
525 therapeutic relevant dose for mice. Nevertheless, recent studies have tried to solve this obstacle by
526 further enlarging the size of the microneedle patch or by utilizing new fabrication strategies to increase
527 maximum loading capacity in a single patch [36, 52]. For instance, Yu et al. increased loading amount of
528 insulin in a patch by increasing the patch size to 5 cm². They showed that the enlarged patch could
529 deliver insulin for controlling glucose level in a minipig model with a weight of 25 kg. It was shown that

530 one microneedle patch could effectively release enough insulin for glucose level regulation within a time
531 period of more than 20 h [17]. In another study, Tran et al. fabricated core-shell microneedles in which
532 the microneedle core was filled with drug suspension or powder to increase drug loading amount. The
533 fabricated microneedles showed a programmed release property of multi-drugs and can release the
534 drugs from a few days to more than a month after a single administration [52]. These new strategies for
535 increasing loading capacity of microneedles could help to promote the translation of microneedle
536 technology.

537 In conclusion, our study showed that polymeric microneedles is a promising transdermal delivery
538 strategy for melittin to improve treatment of RA, by enhancing administration convenience and by
539 modulating release properties of the loaded drug. The sustained release of melittin showed potential to
540 further increase therapeutic efficacy and reduce administration frequency. This study has laid
541 foundation for designing non-invasive and highly potent treatment strategy for RA and other
542 autoimmune diseases.

543 **Acknowledgements**

544 We acknowledge the financial support of the National Natural Science Foundation of China (No.
545 81961130395, No. 82003684), China Postdoctoral Science Foundation Grant (2019M663534), Program
546 of Introducing Talents of Discipline to Universities (Plan 111, No. B18035), and NAF\R1\191217 - Newton
547 Advanced Fellowships 2019.

548 **Conflict of interest:** There is no conflict of interest.

549 **References:**

- 550 [1] J.S. Smolen, D. Aletaha, I.B. McInnes, Rheumatoid arthritis, *The Lancet*, 388 (2016) 2023-2038.
551 [2] B. Combe, R. Landewe, C.I. Daien, C. Hua, D. Aletaha, J.M. Álvaro-Gracia, M. Bakkers, N. Brodin, G.R.
552 Burmester, C. Codreanu, R. Conway, M. Dougados, P. Emery, G. Ferraccioli, J. Fonseca, K. Raza, L. Silva-
553 Fernández, J.S. Smolen, D. Skingle, Z. Szekanecz, T.K. Kvien, A. van der Helm-van Mil, R. van Vollenhoven,
554 2016 update of the EULAR recommendations for the management of early arthritis, *Ann Rheum Dis*, 76
555 (2017) 948-959.
556 [3] D. Aletaha, J.S. Smolen, Diagnosis and Management of Rheumatoid Arthritis: A Review, *Jama*, 320
557 (2018) 1360-1372.
558 [4] W. Wang, H. Zhou, L. Liu, Side effects of methotrexate therapy for rheumatoid arthritis: A systematic
559 review, *European journal of medicinal chemistry*, 158 (2018) 502-516.
560 [5] E. Moroz, S. Matoori, J.C. Leroux, Oral delivery of macromolecular drugs: Where we are after almost
561 100years of attempts, *Advanced drug delivery reviews*, 101 (2016) 108-121.
562 [6] M. Qindeel, M.H. Ullah, D. Fakhar ud, N. Ahmed, A.u. Rehman, Recent trends, challenges and future
563 outlook of transdermal drug delivery systems for rheumatoid arthritis therapy, *Journal of Controlled*
564 *Release*, 327 (2020) 595-615.
565 [7] P. Wu, Q. Liang, P. Feng, C. Li, C. Yang, H. Liang, H. Tang, C. Shuai, A Novel Brucine Gel Transdermal
566 Delivery System Designed for Anti-Inflammatory and Analgesic Activities, *International journal of*
567 *molecular sciences*, 18 (2017).
568 [8] S.F. Ng, L.S. Tan, F. Buang, Transdermal anti-inflammatory activity of bilayer film containing olive
569 compound hydroxytyrosol: physical assessment, in vivo dermal safety and efficacy study in Freund's
570 adjuvant-induced arthritic rat model, *Drug development and industrial pharmacy*, 43 (2017) 108-119.

571 [9] M. Lodzki, B. Godin, L. Rakou, R. Mechoulam, R. Gallily, E. Touitou, Cannabidiol-transdermal delivery
572 and anti-inflammatory effect in a murine model, *Journal of controlled release : official journal of the*
573 *Controlled Release Society*, 93 (2003) 377-387.

574 [10] Y. Gu, X. Tang, M. Yang, D. Yang, J. Liu, Transdermal drug delivery of triptolide-loaded
575 nanostructured lipid carriers: Preparation, pharmacokinetic, and evaluation for rheumatoid arthritis,
576 *International Journal of Pharmaceutics*, 554 (2019) 235-244.

577 [11] Q.D. Pham, S. Björklund, J. Engblom, D. Topgaard, E. Sparr, Chemical penetration enhancers in
578 stratum corneum - Relation between molecular effects and barrier function, *Journal of controlled*
579 *release : official journal of the Controlled Release Society*, 232 (2016) 175-187.

580 [12] K. Ita, Transdermal Delivery of Drugs with Microneedles-Potential and Challenges, *Pharmaceutics*, 7
581 (2015) 90-105.

582 [13] Y.-C. Kim, J.-H. Park, M.R. Prausnitz, Microneedles for drug and vaccine delivery, *Advanced drug*
583 *delivery reviews*, 64 (2012) 1547-1568.

584 [14] G. Du, X. Sun, Current Advances in Sustained Release Microneedles, *Pharmaceutical Fronts*, 02
585 (2020) e11-e22.

586 [15] M. Kirkby, A.R.J. Hutton, R.F. Donnelly, Microneedle Mediated Transdermal Delivery of Protein,
587 Peptide and Antibody Based Therapeutics: Current Status and Future Considerations, *Nature Public*
588 *Health Emergency Collection*, 37.

589 [16] Y. Ye, C. Wang, X. Zhang, Q. Hu, Y. Zhang, Q. Liu, D. Wen, J. Milligan, A. Bellotti, L. Huang, G. Dotti, Z.
590 Gu, A melanin-mediated cancer immunotherapy patch, *Science Immunology*, 2 (2017) eaan5692.

591 [17] J. Yu, J. Wang, Y. Zhang, G. Chen, W. Mao, Y. Ye, A.R. Kahkoska, J.B. Buse, R. Langer, Z. Gu, Glucose-
592 responsive insulin patch for the regulation of blood glucose in mice and minipigs, *Nature Biomedical*
593 *Engineering*, 4 (2020) 499-506.

594 [18] S.D. Gittard, B. Chen, H. Xu, A. Ovsianikov, B.N. Chichkov, N.A. Monteiro-Riviere, R.J. Narayan, The
595 Effects of Geometry on Skin Penetration and Failure of Polymer Microneedles, *Journal of Adhesion*
596 *Science & Technology*, 27 (2013) 227-243.

597 [19] J.H. Park, M.R. Prausnitz, Analysis of Mechanical Failure of Polymer Microneedles by Axial Force,
598 *The journal of the Korean Physical Society*, 56 (2010) 1223-1227.

599 [20] J.H. Park, M.G. Allen, M.R. Prausnitz, Polymer microneedles for controlled-release drug delivery,
600 *Pharmaceutical research*, 23 (2006) 1008-1019.

601 [21] G. Du, Z. Zhang, P. He, Z. Zhang, X. Sun, Determination of the mechanical properties of polymeric
602 microneedles by micromanipulation, *Journal of the mechanical behavior of biomedical materials*, 117
603 (2021) 104384.

604 [22] B.V. Nguyen, Q.G. Wang, N.J. Kuiper, A.J. El Haj, C.R. Thomas, Z. Zhang, Biomechanical properties of
605 single chondrocytes and chondrons determined by micromanipulation and finite-element modelling,
606 *Journal of the Royal Society, Interface*, 7 (2010) 1723-1733.

607 [23] J.-D. Lee, H.-J. Park, Y. Chae, S. Lim, An Overview of Bee Venom Acupuncture in the Treatment of
608 Arthritis, *Evid Based Complement Alternat Med*, 2 (2005) 79-84.

609 [24] Y.B. Kwon, H.J. Lee, H.J. Han, W.C. Mar, S.K. Kang, O.B. Yoon, A.J. Beitz, J.H. Lee, The water-soluble
610 fraction of bee venom produces antinociceptive and anti-inflammatory effects on rheumatoid arthritis in
611 rats, *Life Sciences*, 71 (2002) 191-204.

612 [25] S.-J. Hong, G.S. Rim, H.I. Yang, C.S. Yin, H.G. Koh, M.-H. Jang, C.-J. Kim, B.-K. Choe, J.-H. Chung, Bee
613 venom induces apoptosis through caspase-3 activation in synovial fibroblasts of patients with
614 rheumatoid arthritis, *Toxicon*, 46 (2005) 39-45.

615 [26] Bae, Hyunsu, Lee, Gihyun, Anti-Inflammatory Applications of Melittin, a Major Component of Bee
616 Venom: Detailed Mechanism of Action and Adverse Effects, *Molecules*, (2016).

617 [27] W.F. DeGrado, G.F. Musso, M. Lieber, E.T. Kaiser, F.J. Kézdy, Kinetics and mechanism of hemolysis
618 induced by melittin and by a synthetic melittin analogue, *Biophysical journal*, 37 (1982) 329-338.

619 [28] Y.Q. Ye, J.C. Yu, C. Wang, N.Y. Nguyen, G.M. Walker, J.B. Buse, Z. Gu, Microneedles Integrated with
620 Pancreatic Cells and Synthetic Glucose-Signal Amplifiers for Smart Insulin Delivery, *Adv Mater*, 28 (2016)
621 3115-3121.

622 [29] Li, Jinghua, Ke, Tao, He, Chao, C. o, Wei, Mengqi, Zhang, The Anti-Arthritic Effects of Synthetic
623 Melittin on the Complete Freund's Adjuvant-Induced Rheumatoid Arthritis Model in Rats, *American*
624 *Journal of Chinese Medicine*, (2010).

625 [30] J.D. Lee, S.Y. Kim, T.W. Kim, S.H. Lee, H.I. Yang, D.I. Lee, Y.H. Lee, Anti-inflammatory effect of bee
626 venom on type II collagen-induced arthritis, *The American journal of Chinese medicine*, 32 (2004) 361-
627 367.

628 [31] H.J. Mahdi, N.A.K. Khan, M.Z.B. Asmawi, R. Mahmud, A.L.M. V, In vivo anti-arthritic and anti-
629 nociceptive effects of ethanol extract of *Moringa oleifera* leaves on complete Freund's adjuvant (CFA)-
630 induced arthritis in rats, *Integrative medicine research*, 7 (2018) 85-94.

631 [32] A.J. Gallagher, A.N. Annaidh, K. Bruyère, et al., Dynamic Tensile Properties of Human Skin, in,
632 *International Research Council on the Biomechanics of Injury*, 2012.

633 [33] J.W. Lee, J.H. Park, M.R. Prausnitz, Dissolving microneedles for transdermal drug delivery,
634 *Biomaterials*, 29 (2008) 2113-2124.

635 [34] K. Ita, Dissolving microneedles for transdermal drug delivery: Advances and challenges, *Biomedicine*
636 *& Pharmacotherapy*, 93 (2017) 1116-1127.

637 [35] P. Singh, A. Carrier, Y. Chen, S. Lin, X. Zhang, Polymeric microneedles for controlled transdermal
638 drug delivery, *Journal of Controlled Release*, 315 (2019) 97-113.

639 [36] S. Kim, H. Yang, J. Eum, Y. Ma, S. Fakhraei Lahiji, H. Jung, Implantable powder-carrying microneedles
640 for transdermal delivery of high-dose insulin with enhanced activity, *Biomaterials*, 232 (2020) 119733.

641 [37] J. Yu, Y. Zhang, Z. Gu, Glucose-Responsive Insulin Delivery by Microneedle-Array Patches Loaded
642 with Hypoxia-Sensitive Vesicles, *Methods Mol Biol*, 1570 (2017) 251-259.

643 [38] P.C. Demuth, J.J. Moon, H. Suh, P.T. Hammond, D.J. Irvine, Releasable Layer-by-Layer Assembly of
644 Stabilized Lipid Nanocapsules on Microneedles for Enhanced Transcutaneous Vaccine Delivery, *Acs Nano*,
645 6 (2012) 8041.

646 [39] J. Di, S. Yao, Y. Ye, Z. Cui, J. Yu, T.K. Ghosh, Y. Zhu, Z. Gu, Stretch-Triggered Drug Delivery from
647 Wearable Elastomer Films Containing Therapeutic Depots, *ACS Nano*, 9 (2015) 9407-9415.

648 [40] M.C. Chen, S.F. Huang, K.Y. Lai, M.H. Ling, Fully embeddable chitosan microneedles as a sustained
649 release depot for intradermal vaccination, *Biomaterials*, 34 (2013) 3077-3086.

650 [41] Q. Wang, J. Jiang, W. Chen, H. Jiang, Z. Zhang, X. Sun, Targeted delivery of low-dose dexamethasone
651 using PCL-PEG micelles for effective treatment of rheumatoid arthritis, *Journal of Controlled Release*,
652 230 (2016) 64-72.

653 [42] Q. Wang, Y. Li, X. Chen, H. Jiang, Z. Zhang, X. Sun, Optimized in vivo performance of acid-labile
654 micelles for the treatment of rheumatoid arthritis by one single injection, *Nano research*, (2019).

655 [43] Q. Wang, H. Jiang, Y. Li, W. Chen, H. Li, K. Peng, Z. Zhang, X. Sun, Targeting NF- κ B signaling with
656 polymeric hybrid micelles that co-deliver siRNA and dexamethasone for arthritis therapy, *Biomaterials*,
657 122 (2017) 10-22.

658 [44] H.J. Park, S.H. Lee, D.J. Son, K.W. Oh, K.H. Kim, H.S. Song, G.J. Kim, G.T. Oh, D.Y. Yoon, J.T. Hong,
659 Antiarthritic effect of bee venom: inhibition of inflammation mediator generation by suppression of NF-
660 κ B through interaction with the p50 subunit, *Arthritis and rheumatism*, 50 (2004) 3504-3515.

661 [45] F.A.H. Cooles, J.D. Isaacs, A.E. Anderson, Treg Cells in Rheumatoid Arthritis: An Update, *Current*
662 *Rheumatology Reports*, 15 (2013) 352.

663 [46] J. Li, T. Ke, C. He, W. Cao, M. Wei, L. Zhang, J.-X. Zhang, W. Wang, J. Ma, Z.-R. Wang, Z.-J. Shao, The
664 Anti-Arthritic Effects of Synthetic Melittin on the Complete Freund's Adjuvant-Induced Rheumatoid
665 Arthritis Model in Rats, *The American Journal of Chinese Medicine*, 38 (2010) 1039-1049.

- 666 [47] G. Lee, H. Bae, Anti-Inflammatory Applications of Melittin, a Major Component of Bee Venom:
667 Detailed Mechanism of Action and Adverse Effects, *Molecules*, 21 (2016) 616.
- 668 [48] J.A. Lee, M.J. Son, J. Choi, J.H. Jun, J.-I. Kim, M.S. Lee, Bee venom acupuncture for rheumatoid
669 arthritis: a systematic review of randomised clinical trials, *BMJ Open*, 4 (2014) e006140.
- 670 [49] X. Chen, H. Fan, J. Chen, H. Fan, P. Wu, Bee venom acupuncture for adhesive capsulitis: A protocol
671 for systematic review and meta-analysis, *Medicine*, 99 (2020).
- 672 [50] M.T. Tosteson, S.J. Holmes, M. Razin, D.C. Tosteson, Melittin lysis of red cells, *The Journal of*
673 *membrane biology*, 87 (1985) 35-44.
- 674 [51] H. Zarrinahad, A. Mahmoodzadeh, M.P. Hamidi, M. Mahdavi, A. Moradi, K.P. Bagheri, D.
675 Shahbazzadeh, Apoptotic Effect of Melittin Purified from Iranian Honey Bee Venom on Human Cervical
676 Cancer HeLa Cell Line, *International Journal of Peptide Research and Therapeutics*, 24 (2018) 563-570.
- 677 [52] K.T.M. Tran, T.D. Gavitt, N.J. Farrell, E.J. Curry, A.B. Mara, A. Patel, L. Brown, S. Kilpatrick, R.
678 Piotrowska, N. Mishra, S.M. Szczepanek, T.D. Nguyen, Transdermal microneedles for the programmable
679 burst release of multiple vaccine payloads, *Nature Biomedical Engineering*, (2020).

680